Supporting Information

Blue-Emitting Bis-tridentate Ir(III) Phosphors: OLED Performances vs. Substituent Effects

Hsin-Hung Kuo, Ling-Yang Hsu, Jen-Yung Tso, Wen-Yi Hung,* Shih-Hung Liu, Pi-Tai Chou,* Ken-Tsung Wong, Ze-lin Zhu, Chun-Sing Lee, Alex K.-Y. Jen,* and Yun Chi*

Hsin-Hung Kuo, Ling-Yang Hsu, Prof. Yun Chi

Department of Chemistry and Frontier Research Center on Fundamental and Applied Sciences of Matters, National Tsing Hua University, Hsinchu 30013, Taiwan.

Jen-Yung Tso, Prof. Wen-Yi Hung

Institute of Optoelectronic Sciences, National Taiwan Ocean University, Keelung 20224, Taiwan.

Dr. Shih-Hung Liu, Prof. Pi-Tai Chou, Prof. Ken-Tsung Wong

Department of Chemistry and Instrumentation Center, National Taiwan University, Taipei 10617, Taiwan.

Ze-lin Zhu, Prof. Chun-Sing Lee,

Center of Super-Diamond and Advanced Films (COSDAF) and Department of Chemistry, City University of Hong Kong, Hong Kong SAR.

Prof. Alex K.-Y. Jen, Prof. Yun Chi

Department of Materials Science and Engineering and Department of Chemistry, City University of Hong Kong, Hong Kong SAR.

Experimental section:

General information:

Electrochemistry: Cyclic voltammetry was conducted on a CHI621A Electrochemical Analyzer, equipped with a Ag/Ag^+ reference electrode. The oxidation and reduction potentials were measured using a platinum working electrode with 0.1 M of [NBu_4PF_6] in CH_2Cl_2 and a gold wire with 0.1M of [NBu_4PF_6] in THF, respectively. The potentials were referenced externally to the ferrocenium/ferrocene (Fc^+/Fc) couple.

Photophysical measurements: UV-Vis spectra were recorded on a HITACHI U-3900 spectrophotometer. The steady-state emission spectra and lifetime studies were measured with Edinburgh FL 900 photon-counting system. Both wavelength-dependent excitation and emission responses of the fluorimeter were calibrated. Spectral grade solvents (Merck) were used as received. To determine the photoluminescence quantum yield in solution, samples were degassed using at least three freeze-pump-thaw cycles. The solution quantum yields are calculated using the standard sample which has a known quantum yield, according to the following equation

$$\Phi = \Phi_R \frac{I}{I_R}\frac{A_R}{A}\frac{\eta^2}{\eta_R^2}$$

where Φ is the quantum yield, the subscript R refers to the reference compound of known quantum yield, I is the integrated fluorescence intensity and η is the refractive index of the solvent. A is the absorbance at the excitation wavelength with the value of absorbance between 0.02 ~ 0.05.

Lifetime studies were performed by an Edinburgh FL 900 time correlated single photon counting (TCSPC) system with an EPL-375 diode laser as the excitation source. Data were analyzed using a nonlinear least-squares procedure in combination with an iterative convolution method. The emission decays were fitted by the sum of exponential functions with a temporal resolution of ~ 300 ps after the deconvolution of instrument response function.

Computational Method.

All calculations were performed with the Gaussian 09 program package.[1] The geometry optimization of ground states of the six Ir(III) complexes are simulated with density functional theory (DFT) at the hybrid functional PBE1PBE/LANL2DZ (Ir) and PBE1PBE/6-31g(d,p) (H, C, N, F) levels using CH_2Cl_2 as the solvent. The optimized structures of the six Ir(III) complexes are then used to calculate the five lowest singlet ($S_0 \rightarrow S_5$) and triplet optical electronic transitions ($S_0 \rightarrow T_5$) using the time–dependent density functional theory (TD–DFT) method. The solvent effect is based on the polarizable continuum model (PCM), which is supported implemented in the Gaussian 09 program. For both singlet and triplet optical transitions Mulliken population analysis (MPA) is applied to obtain the electron density distribution of each atom in specific molecular orbital of the Ir(III) complexes as well as to calculate the metal-to-ligand charge transfer (MLCT) in each assignment during the singlet and triplet optical transitions.

OLED Device Fabrication

All chemicals were purified through vacuum sublimation prior to use. The OLEDs were fabricated through vacuum deposition of the materials at 10^{-6} Torr onto the ITO-coated glass substrates having a sheet resistance of 15 Ω sq^{-1}. Prior to use the ITO surface was cleaned ultrasonically; i.e. with acetone, methanol, and deionized water in sequence and finally with UV-ozone. The deposition rate of each organic material was ca. 1–2 Å s^{-1}. The *J–V–L* characteristics of the devices were measured simultaneously in a glove-box using a Keithley 2614B source meter equipped with a calibration Si-photodiode. EL spectra were measured using a photodiode array (Ocean Optics USB2000+).

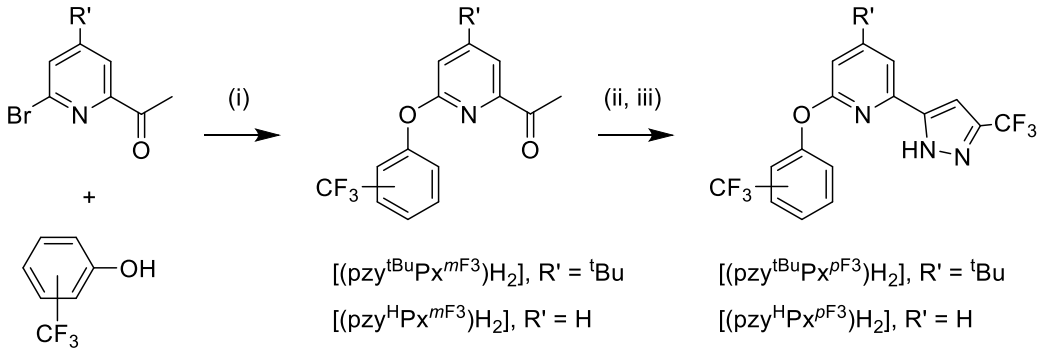

Scheme S1. Synthetic procedure for the dianionic chromophoric chelates LH_2. Experimental conditions: (i) picolinic acid, CuI, DMSO, K_3PO_4; (ii) NaOEt, CF_3CO_2Et, THF, reflux; (iii) N_2H_4, EtOH, reflux.

In **Tables S1 to S6** we have calculated both $S_0 \rightarrow T_1$ and $T_1 \rightarrow S_0$ transition properties based on geometry optimized S_0 and T_1, respectively. As for the emission properties it is more appropriate to apply the calculation of $T_1 \rightarrow S_0$ transition to compare with the experimental results, as elaborated in the text.

Table S1(a). The calculated wavelengths, transition probabilities and charge transfer character of the optical absorptions for Ir(III) complex **Px-11** in CH_2Cl_2.

State	λ (nm)	f	Assignments	MLCT
T_1	409.3	0	HOMO-3→LUMO(49%) HOMO-2→LUMO(17%) HOMO-2→LUMO+1(16%) HOMO-3→LUMO+1(5%)	16.49%
T_2	384	0	HOMO-1→LUMO+3(31%) HOMO-4→LUMO+2(18%) HOMO-1→LUMO+2(14%) HOMO-1→LUMO+6(10%) HOMO→LUMO+2(7%)	13.23%
T_3	371.3	0	HOMO-2→LUMO(27%) HOMO-2→LUMO+1(17%) HOMO→LUMO+1(14%) HOMO→LUMO(8%) HOMO→LUMO+4(5%)	18.24%
T_4	358.4	0	HOMO→LUMO(77%)	26.16%
T_5	351.1	0	HOMO-2→LUMO(42%) HOMO-3→LUMO(11%) HOMO→LUMO+4(8%)	12.84%
S_1	341.3	0.0102	HOMO→LUMO(97%)	32.95%
S_2	330.9	0.0049	HOMO-1→LUMO(97%)	25.32%
S_3	319.7	0.1657	HOMO-2→LUMO(88%)	17.08%
S_4	296.6	0.0441	HOMO→LUMO+1(88%)	31.40%
S_5	293.9	0.0051	HOMO→LUMO+3(55%) HOMO-1→LUMO+2(27%) HOMO-1→LUMO+3(7%)	21.45%

Table S1(b). The calculated wavelengths, transition probabilities and charge transfer character of the lowest emission for Ir(III) complex **PX-11** in CH_2Cl_2.

State	λ (nm)	f	Assignments	MLCT
$T_1 \rightarrow S_0$	546.3	0	LUMO→HOMO-2(73%) LUMO→HOMO-3(16%)	8.45%
$S_1 \rightarrow S_0$	433.4	0.0159	LUMO→HOMO(99%)	30.12%

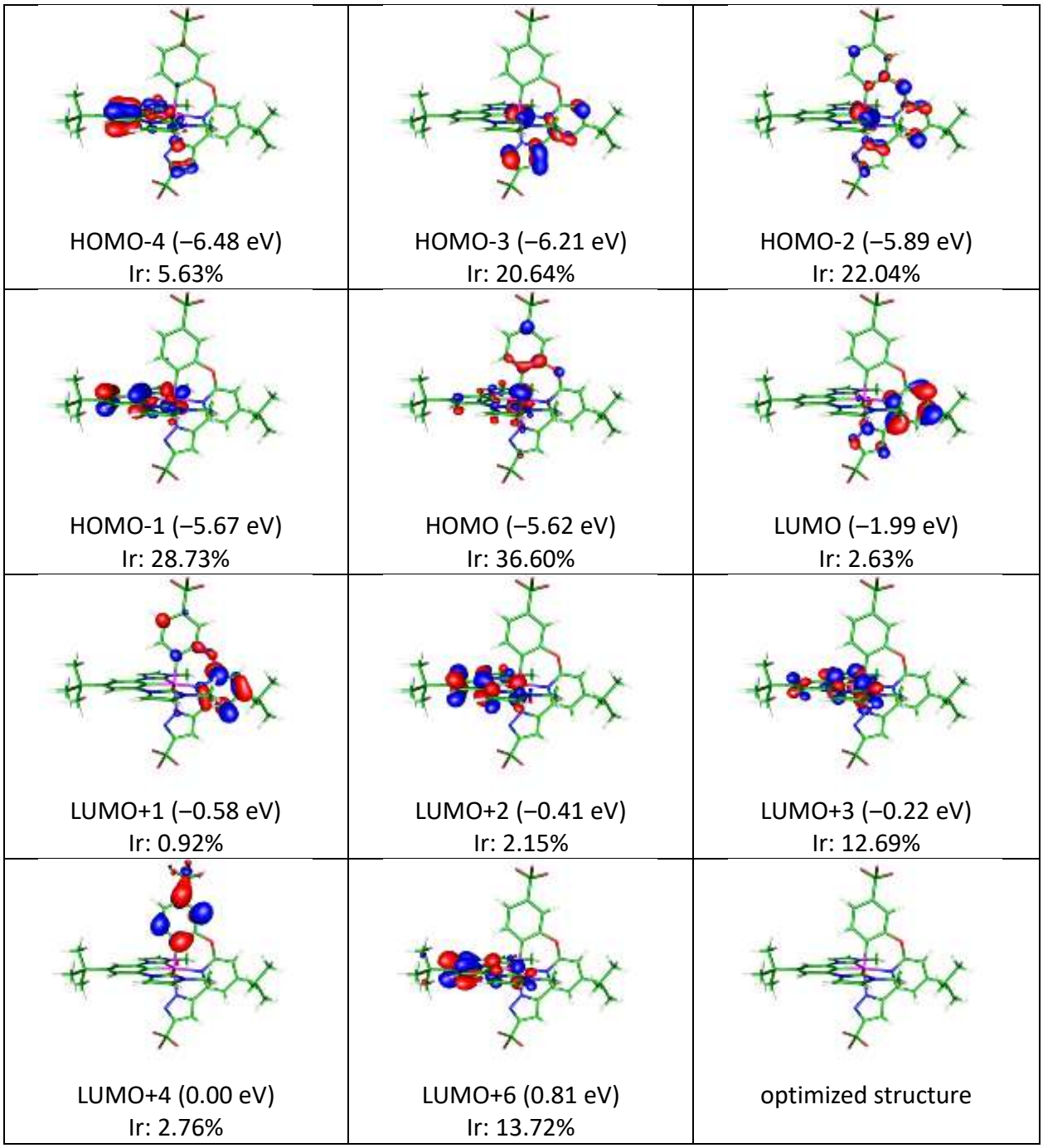

Figure S1(a). Frontier molecular orbitals pertinent to the absorptions for the ground state S_0 of Ir(III) complex **Px-11**. The electron density distributions of Ir atom in each molecular orbital are showed. For the clarity of viewing, the optimized structure with no involvement of frontier orbitals is shown at the last figure.

 HOMO-3 (–6.11 eV) Ir: 35.65%	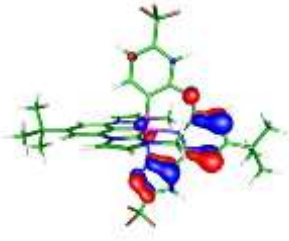 HOMO-2 (–5.77 eV) Ir: 6.26%	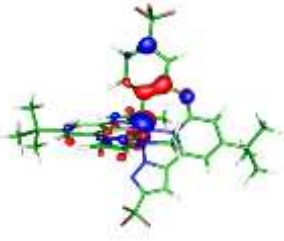 HOMO (–5.65 eV) Ir: 34.69%
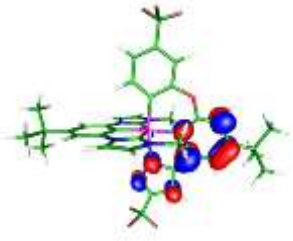 LUMO (–1.45 eV) Ir: 2.05%	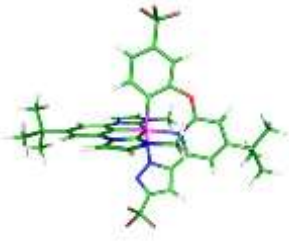 optimized structure	

Figure S1(b). Frontier molecular orbitals pertinent to the emission for the excited state T_1 of Ir(III) complex **Px-11**. The electron density distributions of Ir atom in each molecular orbital are showed. For the clarity of viewing, the optimized structure with no involvement of frontier orbitals is shown at the last figure.

Table S2(a). The calculated wavelengths, transition probabilities and charge transfer character of the optical absorptions for Ir(III) complex **Px-12** in CH_2Cl_2.

State	λ (nm)	f	Assignments	MLCT
T_1	418.7	0	HOMO-3→LUMO(54%) HOMO-2→LUMO(20%) HOMO-2→LUMO+1(10%)	15.50%
T_2	384.9	0	HOMO-1→LUMO+3(37%) HOMO-4→LUMO+2(18%) HOMO→LUMO+2(16%) HOMO-1→LUMO+6(11%)	13.52%
T_3	376.1	0	HOMO→LUMO(25%) HOMO-2→LUMO(24%) HOMO-2→LUMO+1(17%) HOMO→LUMO+1(11%)	20.42%
T_4	367.4	0	HOMO→LUMO(62%) HOMO-2→LUMO(10%) HOMO-4→LUMO(5%)	22.90%
T_5	355.4	0	HOMO-2→LUMO(35%) HOMO-3→LUMO(16%) HOMO→LUMO+4(9%)	12.60%
S_1	351.2	0.0097	HOMO→LUMO(96%)	32.19%
S_2	339	0.0004	HOMO-1→LUMO(96%)	24.88%
S_3	325.1	0.1407	HOMO-2→LUMO(89%)	17.17%
S_4	296.6	0.0578	HOMO→LUMO+1(77%) HOMO-3→LUMO(16%)	29.87%
S_5	296.4	0.0054	HOMO→LUMO+3(78%) HOMO-1→LUMO+2(10%) HOMO→LUMO+2(7%)	32.43%

Table S2(b). The calculated wavelengths, transition probabilities and charge transfer character of the lowest emission for Ir(III) complex **Px-12** in CH_2Cl_2.

State	λ (nm)	f	Assignments	MLCT
$T_1 \rightarrow S_0$	561.9	0	LUMO→HOMO-2(74%) LUMO→HOMO-3(18%)	8.39%
$S_1 \rightarrow S_0$	445.3	0.0138	LUMO→HOMO(99%)	29.90%

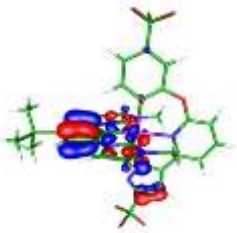 HOMO-4 (–6.51 eV) Ir: 6.19%	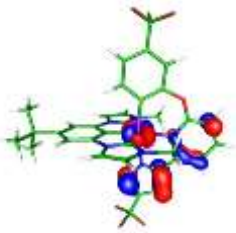 HOMO-3 (–6.23 eV) Ir: 20.33%	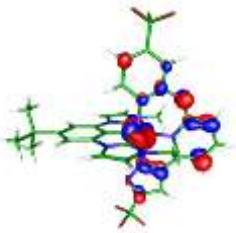 HOMO-2 (–5.91 eV) Ir: 21.93%
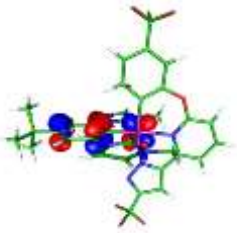 HOMO-1 (–5.69 eV) Ir: 28.56%	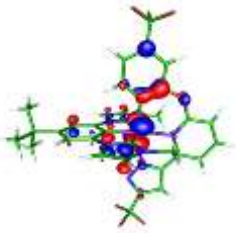 HOMO (–5.63 eV) Ir: 36.17%	 LUMO (–2.10 eV) Ir: 2.64%
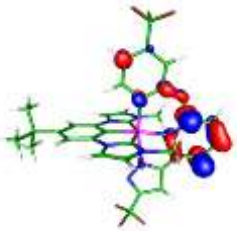 LUMO+1 (–0.58 eV) Ir: 1.06%	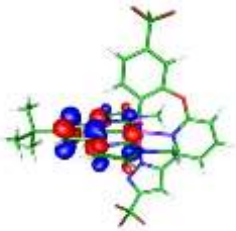 LUMO+2 (–0.43 eV) Ir: 2.03%	 LUMO+3 (–0.28 eV) Ir: 13.33%
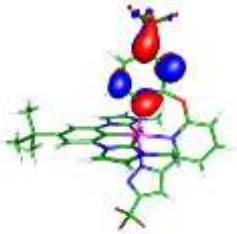 LUMO+4 (–0.01 eV) Ir: 2.61%	 LUMO+6 (0.77 eV) Ir: 13.37%	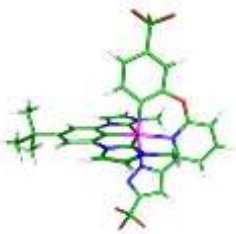 optimized structure

Figure S2(a). Frontier molecular orbitals pertinent to the absorptions for the ground state S_0 of Ir(III) complex **Px-12**. The electron density distributions of Ir atom in each molecular orbital are showed. For the clarity of viewing, the optimized structure with no involvement of frontier orbitals is shown at the last figure.

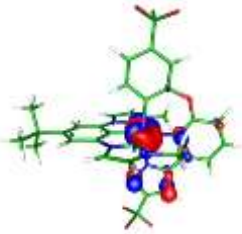 HOMO-3 (–6.13 eV) Ir: 35.17%	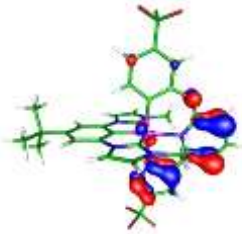 HOMO-2 (–5.81 eV) Ir: 5.51%	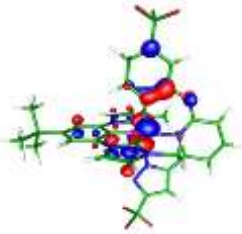 HOMO (–5.66 eV) Ir: 34.88%
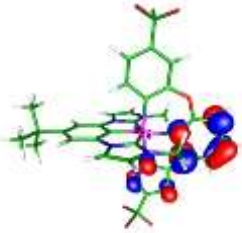 LUMO (–1.55 eV) Ir: 2.19%	 optimized structure	

Figure S2(b). Frontier molecular orbitals pertinent to the emission for the excited state T_1 of Ir(III) complex **Px-12**. The electron density distributions of Ir atom in each molecular orbital are showed. For the clarity of viewing, the optimized structure with no involvement of frontier orbitals is shown at the last figure.

Table S3(a). The calculated wavelengths, transition probabilities and charge transfer character of the optical absorptions for Ir(III) complex **Px-13** in CH_2Cl_2.

State	λ (nm)	f	Assignments	MLCT
T_1	409.7	0	HOMO-3→LUMO(49%) HOMO-2→LUMO+1(17%) HOMO-2→LUMO(14%) HOMO-3→LUMO+1(7%)	12.04%
T_2	384	0	HOMO-1→LUMO+3(34%) HOMO-4→LUMO+2(18%) HOMO→LUMO+2(11%) HOMO-1→LUMO+6(11%) HOMO-1→LUMO+2(10%)	14.17%
T_3	375.5	0	HOMO-2→LUMO(28%) HOMO-2→LUMO+1(16%) HOMO→LUMO+1(14%) HOMO→LUMO(13%) HOMO-6→LUMO+4(7%) HOMO→LUMO+5(6%)	20.98%
T_4	360.5	0	HOMO→LUMO(75%) HOMO-2→LUMO(6%)	27.28%
T_5	350.4	0	HOMO-2→LUMO(40%) HOMO-3→LUMO(12%) HOMO→LUMO+5(8%) HOMO-6→LUMO+4(7%)	12.92%
S_1	344.5	0.0105	HOMO→LUMO(97%)	33.72%
S_2	333	0.0035	HOMO-1→LUMO(98%)	25.11%
S_3	320.4	0.1571	HOMO-2→LUMO(87%) HOMO→LUMO+1(5%)	19.43%
S_4	302	0.0543	HOMO→LUMO+1(90%)	33.02%
S_5	294.9	0.0069	HOMO→LUMO+3(63%) HOMO-1→LUMO+2(18%) HOMO→LUMO+2(11%)	24.21%

Table S3(b). The calculated wavelengths, transition probabilities and charge transfer character of the lowest emission for Ir(III) complex **Px-13** in CH_2Cl_2.

State	λ (nm)	f	Assignments	MLCT
$T_1 \rightarrow S_0$	545.8	0	LUMO→HOMO-2(76%) LUMO→HOMO-3(16%)	7.55%
$S_1 \rightarrow S_0$	437	0.0122	LUMO→HOMO(99%)	30.75%

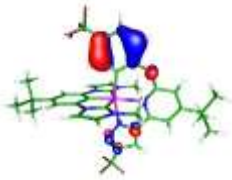 HOMO-6 (–6.88 eV) Ir: 1.54%	 HOMO-4 (–6.47 eV) Ir: 5.88%	 HOMO-3 (–6.21 eV) Ir: 19.63%
 HOMO-2 (–5.89 eV) Ir: 22.98%	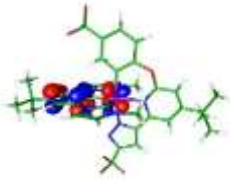 HOMO-1 (–5.66 eV) Ir: 28.37%	 HOMO (–5.60 eV) Ir: 37.51%
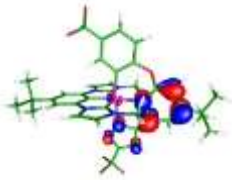 LUMO (–2.00 eV) Ir: 2.75%	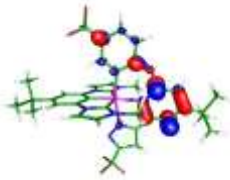 LUMO+1 (–0.65 eV) Ir: 0.82%	 LUMO+2 (–0.40 eV) Ir: 2.17%
 LUMO+3 (–0.21 eV) Ir: 12.74%	 LUMO+4 (0.15 eV) Ir: 0.72%	 LUMO+5 (0.43 eV) Ir: 3.16%
 LUMO+6 (0.82 eV) Ir: 13.10%	 optimized structure	

Figure S3(a). Frontier molecular orbitals pertinent to the absorptions for the ground state S_0 of Ir(III) complex **Px-13**. The electron density distributions of Ir atom in each molecular orbital are showed. For the clarity of viewing, the optimized structure with no involvement of frontier orbitals is shown at the last figure.

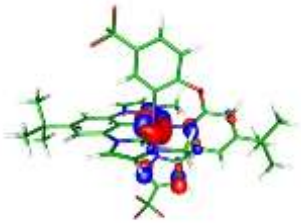 HOMO-3 (–6.11 eV) Ir: 36.11%	 HOMO-2 (–5.77 eV) Ir: 4.85%	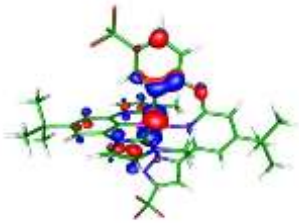 HOMO (–5.63 eV) Ir: 36.54%
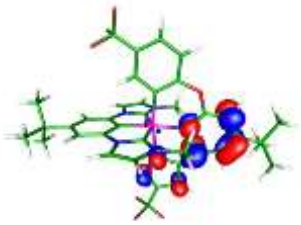 LUMO (–1.45 eV) Ir: 2.08%	 optimized structure	

Figure S3(b). Frontier molecular orbitals pertinent to the emission for the excited state T_1 of Ir(III) complex **Px-13**. The electron density distributions of Ir atom in each molecular orbital are showed. For the clarity of viewing, the optimized structure with no involvement of frontier orbitals is shown at the last figure.

Table S4(a). The calculated wavelengths, transition probabilities and charge transfer character of the optical absorptions for Ir(III) complex **Px-14** in CH_2Cl_2.

State	λ (nm)	f	Assignments	MLCT
T_1	417	0	HOMO-3→LUMO(56%) HOMO-2→LUMO(15%) HOMO-2→LUMO+1(12%) HOMO-3→LUMO+1(6%)	15.46%
T_2	384.1	0	HOMO-1→LUMO+3(32%) HOMO-4→LUMO+2(18%) HOMO-1→LUMO+2(12%) HOMO-1→LUMO+6(10%) HOMO→LUMO+2(9%)	13.53%
T_3	379	0	HOMO→LUMO(34%) HOMO-2→LUMO(22%) HOMO-2→LUMO+1(14%) HOMO→LUMO+1(10%)	23.02%
T_4	370.2	0	HOMO→LUMO(52%) HOMO-2→LUMO(18%) HOMO-4→LUMO(6%)	21.86%
T_5	355.3	0	HOMO-2→LUMO(29%) HOMO-3→LUMO(11%) HOMO→LUMO+5(9%) HOMO-6→LUMO+4(8%) HOMO→LUMO+1(7%) HOMO-1→LUMO(6%)	14.81%
S_1	354.8	0.0093	HOMO→LUMO(97%)	33.48%
S_2	342.5	0.0036	HOMO-1→LUMO(98%)	24.86%
S_3	324.9	0.132	HOMO-2→LUMO(89%)	18.21%
S_4	301.8	0.0429	HOMO→LUMO+1(89%)	32.44%
S_5	296.2	0.1747	HOMO-3→LUMO(84%)	12.99%

Table S4(b). The calculated wavelengths, transition probabilities and charge transfer character of the lowest emission for Ir(III) complex **Px-14** in CH_2Cl_2.

State	λ (nm)	f	Assignments	MLCT
$T_1 \rightarrow S_0$	559.7	0	LUMO→HOMO-2(75%) LUMO→HOMO-3(18%)	7.67%
$S_1 \rightarrow S_0$	451.3	0.107	LUMO→HOMO(99%)	30.52%

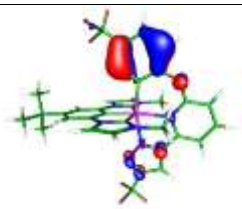 HOMO-6 (–6.91 eV) Ir: 1.25%	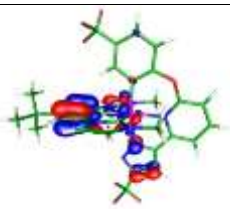 HOMO-4 (–6.49 eV) Ir: 6.62%	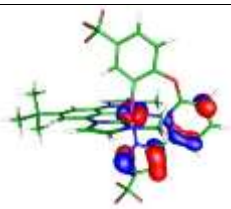 HOMO-3 (–6.24 eV) Ir: 18.26%
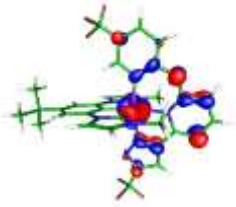 HOMO-2 (–5.95 eV) Ir: 23.26%	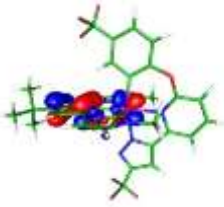 HOMO-1 (–5.68 eV) Ir: 28.17%	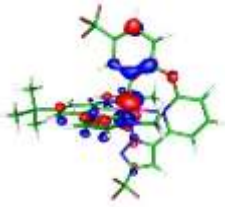 HOMO (–5.62 eV) Ir: 37.32%
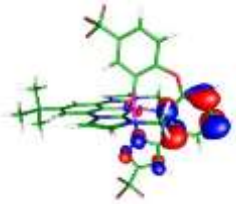 LUMO (–2.13 eV) Ir: 2.80%	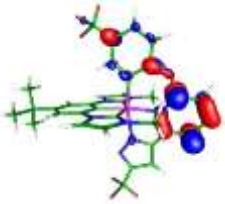 LUMO+1 (–0.66 eV) Ir: 0.87%	 LUMO+2 (–0.42 eV) Ir: 2.16%
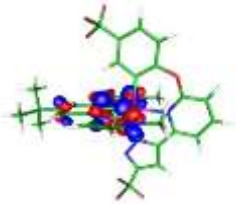 LUMO+3 (–0.23 eV) Ir: 12.73%	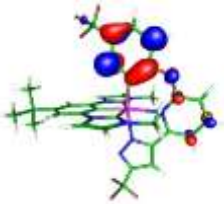 LUMO+4 (0.14 eV) Ir: 0.74%	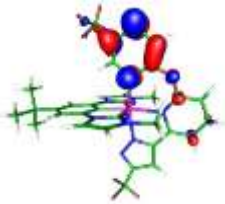 LUMO+5 (0.39 eV) Ir: 3.34%
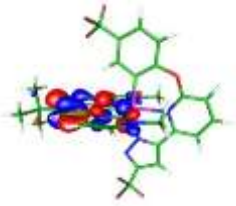 LUMO+6 (0.81 eV) Ir: 13.14%	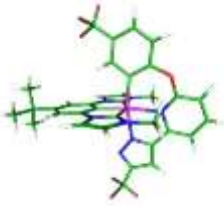 optimized structure	

Figure S4(a). Frontier molecular orbitals pertinent to the absorptions for the ground state S_0 of Ir(III) complex **Px-14**. The electron density distributions of Ir atom in each molecular orbital are showed. For the clarity of viewing, the optimized structure with no involvement of frontier orbitals is shown at the last figure.

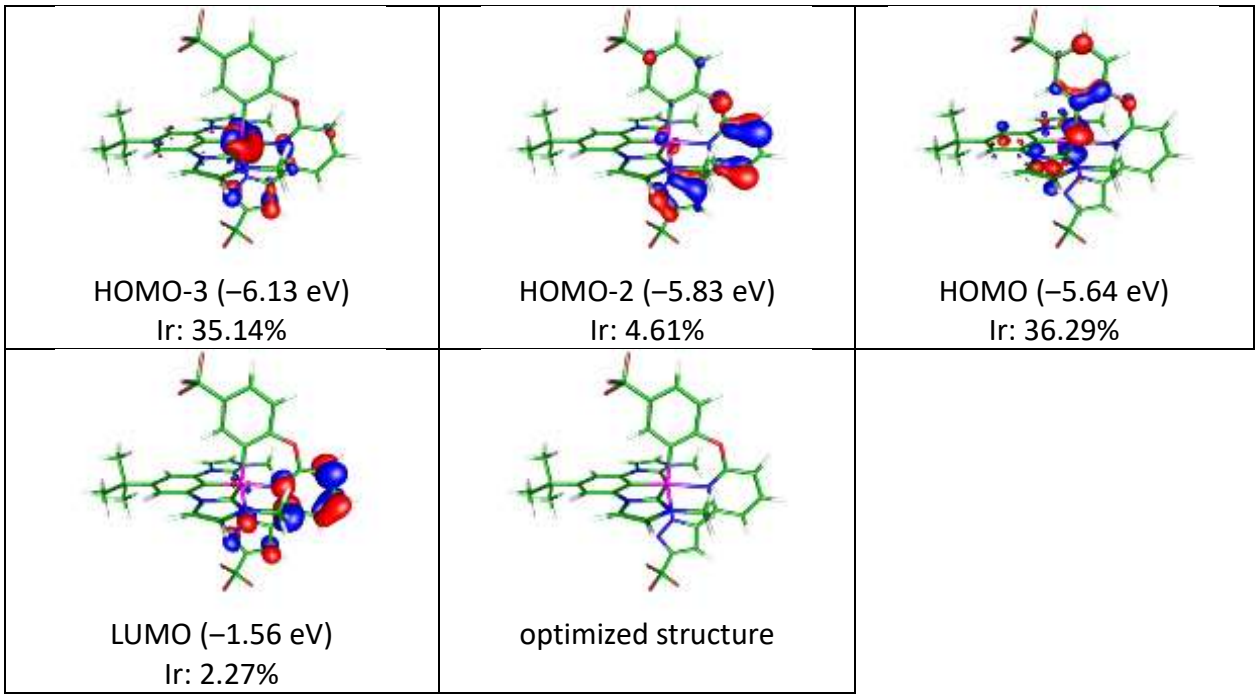

Figure S4(b). Frontier molecular orbitals pertinent to the emission for the excited state T_1 of Ir(III) complex **Px-14**. The electron density distributions of Ir atom in each molecular orbital are showed. For the clarity of viewing, the optimized structure with no involvement of frontier orbitals is shown at the last figure.

Table S5(a). The calculated wavelengths, transition probabilities and charge transfer character of the optical absorptions for Ir(III) complex **Px-15** in CH_2Cl_2.

State	λ (nm)	f	Assignments	MLCT
T_1	418.7	0	HOMO-3→LUMO(55%) HOMO-2→LUMO(16%) HOMO-2→LUMO+1(12%) HOMO-3→LUMO+1(6%)	15.40%
T_2	383.5	0	HOMO-1→LUMO+3(36%) HOMO-4→LUMO+2(18%) HOMO→LUMO+2(16%) HOMO-1→LUMO+6(9%)	13.97%
T_3	381.8	0	HOMO→LUMO(32%) HOMO-2→LUMO(22%) HOMO-2→LUMO+1(15%) HOMO→LUMO+1(8%)	21.40%
T_4	372.3	0	HOMO→LUMO(51%) HOMO-2→LUMO(19%) HOMO-4→LUMO(6%)	21.38%
S_1	356.8	0.0105	HOMO→LUMO(95%)	32.21%
T_5	355.1	0	HOMO-2→LUMO(33%) HOMO-3→LUMO(14%) HOMO-6→LUMO+4(8%) HOMO→LUMO+5(8%) HOMO→LUMO+1(6%)	13.65%
S_2	345.2	0.0002	HOMO-1→LUMO(95%)	24.57%
S_3	326.9	0.1229	HOMO-2→LUMO(88%)	17.56%
S_4	303.7	0.0428	HOMO→LUMO+1(87%)	31.22%
S_5	296.9	0.1742	HOMO-3→LUMO(87%)	13.49%

Table S5(b). The calculated wavelengths, transition probabilities and charge transfer character of the lowest emission for Ir(III) complex **Px-15** in CH_2Cl_2.

State	λ (nm)	f	Assignments	MLCT
$T_1 \rightarrow S_0$	557.3	0	LUMO→HOMO-2(74%) LUMO→HOMO-3(18%)	7.30%
$S_1 \rightarrow S_0$	454.8	0.0101	LUMO→HOMO(99%)	30.87%

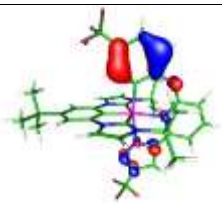 HOMO-6 (–6.90 eV) Ir: 1.31%	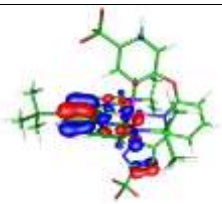 HOMO-4 (–6.47 eV) Ir: 7.79%	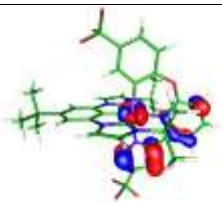 HOMO-3 (–6.24 eV) Ir: 18.33%
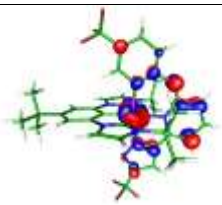 HOMO-2 (–5.93 eV) Ir: 22.78%	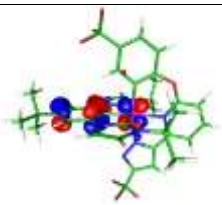 HOMO-1 (–5.66 eV) Ir: 28.69%	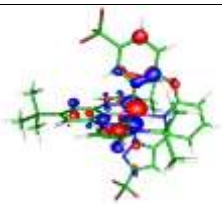 HOMO (–5.61 eV) Ir: 36.74%
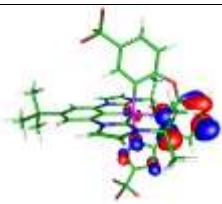 LUMO (–2.13 eV) Ir: 2.83%	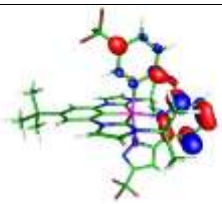 LUMO+1 (–0.67 eV) Ir: 0.86%	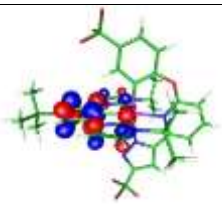 LUMO+2 (–0.39 eV) Ir: 1.78%
 LUMO+3 (–0.17 eV) Ir: 12.33%	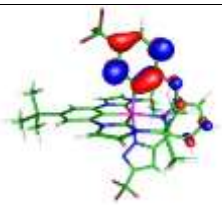 LUMO+4 (0.15 eV) Ir: 0.79%	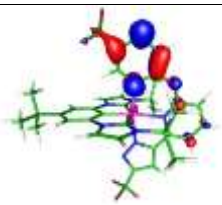 LUMO+5 (0.42 eV) Ir: 2.97%
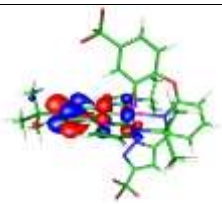 LUMO+6 (0.86 eV) Ir: 13.07%	 optimized structure	

Figure S5(a). Frontier molecular orbitals pertinent to the absorptions for the ground state S_0 of Ir(III) complex **Px-15**. The electron density distributions of Ir atom in each molecular orbital are showed. For the clarity of viewing, the optimized structure with no involvement of frontier orbitals is shown at the last figure.

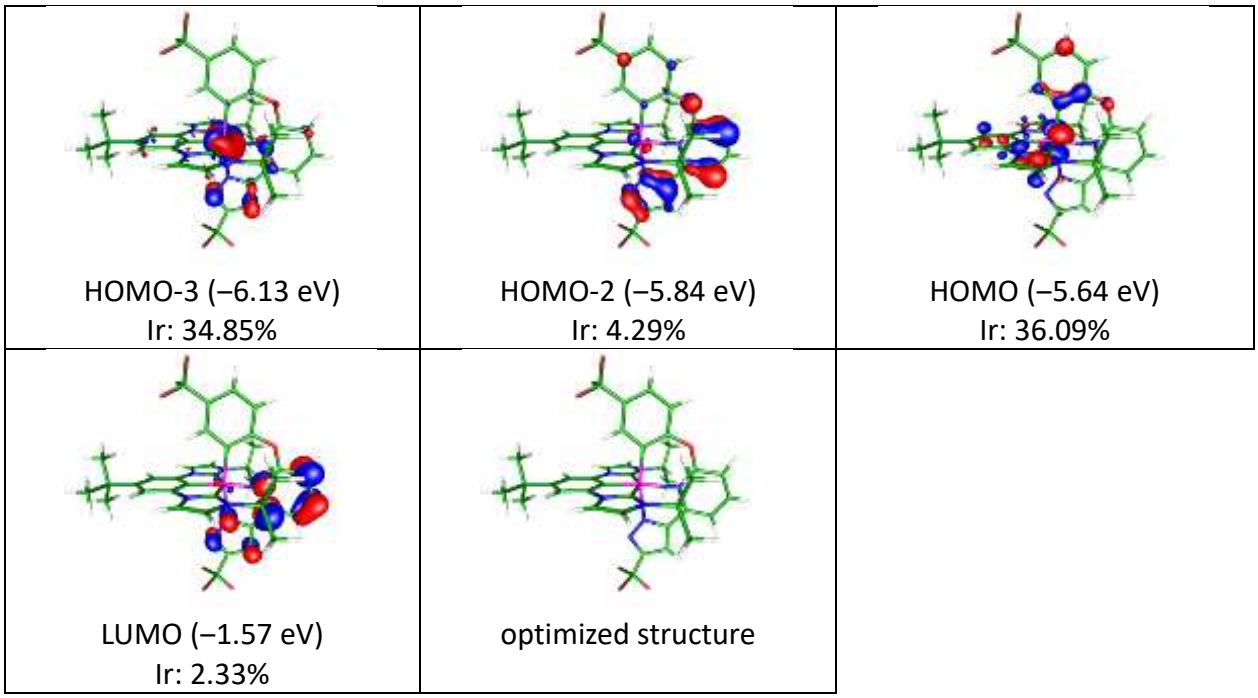

Figure S5(b). Frontier molecular orbitals pertinent to the emission for the excited state T_1 of Ir(III) complex **Px-15**. The electron density distributions of Ir atom in each molecular orbital are showed. For the clarity of viewing, the optimized structure with no involvement of frontier orbitals is shown at the last figure.

Table S6(a). The calculated wavelengths, transition probabilities and charge transfer character of the optical absorptions for Ir(III) complex **Px-16** in CH_2Cl_2.

State	λ (nm)	f	Assignments	MLCT
T_1	418	0	HOMO-3→LUMO(52%) HOMO-2→LUMO(19%) HOMO-2→LUMO+1(12%) HOMO-3→LUMO+1(5%)	15.23%
T_2	384	0	HOMO-1→LUMO+3(21%) HOMO-4→LUMO+2(16%) HOMO→LUMO+2(14%) HOMO-1→LUMO+5(10%)	12.57%
T_3	380.6	0	HOMO→LUMO(29%) HOMO-2→LUMO(22%) HOMO-2→LUMO+1(17%) HOMO→LUMO+1(10%)	20.92%
T_4	370.1	0	HOMO→LUMO(58%) HOMO-2→LUMO(16%) HOMO-4→LUMO(6%)	22.91%
S_1	354.1	0.0119	HOMO→LUMO(95%)	32.12%
T_5	353.6	0	HOMO-2→LUMO(32%) HOMO-3→LUMO(14%) HOMO→LUMO+1(6%)	10.32%
S_2	344	0.0005	HOMO-1→LUMO(96%)	24.02%
S_3	325.5	0.1241	HOMO-2→LUMO(88%)	16.29%
S_4	301.4	0.0442	HOMO→LUMO+1(87%)	31.07%
S_5	295.9	0.1496	HOMO-3→LUMO(86%)	13.83%

Table S6(b). The calculated wavelengths, transition probabilities and charge transfer character of the lowest emission for Ir(III) complex **Px-16** in CH_2Cl_2.

State	λ (nm)	f	Assignments	MLCT
$T_1 \rightarrow S_0$	558.9	0	LUMO→HOMO-2(75%) LUMO→HOMO-3(18%)	7.30%
$S_1 \rightarrow S_0$	453.7	0.0114	LUMO→HOMO(99%)	30.26%

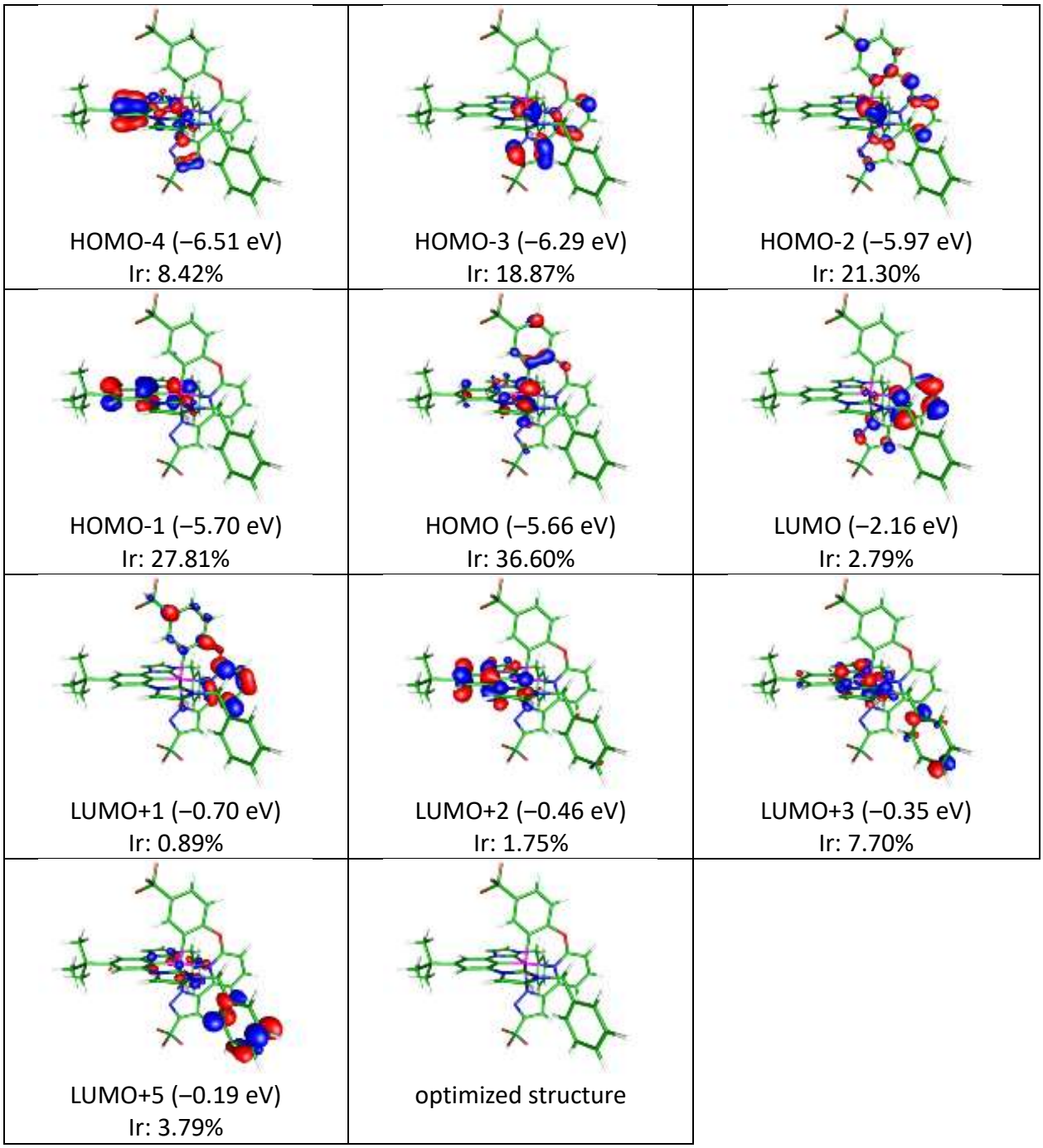

Figure S6(a). Frontier molecular orbitals pertinent to the absorptions for the ground state S_0 of Ir(III) complex **Px-16**. The electron density distributions of Ir atom in each molecular orbital are showed. For the clarity of viewing, the optimized structure with no involvement of frontier orbitals is shown at the last figure.

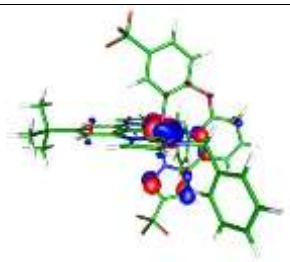

HOMO-3 (–6.18 eV)
Ir: 33.96%

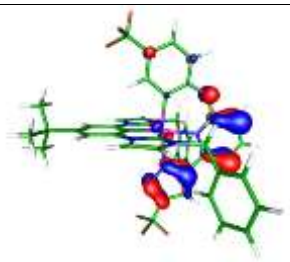

HOMO-2 (–5.87 eV)
Ir: 4.49%

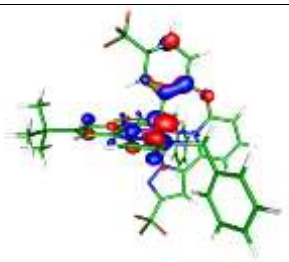

HOMO (–5.69 eV)
Ir: 35.31%

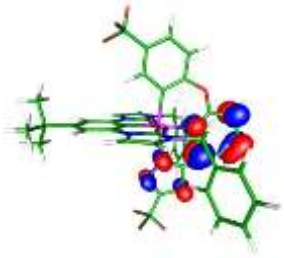

LUMO (–1.60 eV)
Ir: 2.34%

optimized structure

Figure S6(b). Frontier molecular orbitals pertinent to the emission for the excited state T_1 of Ir(III) complex **Px-16**. The electron density distributions of Ir atom in each molecular orbital are showed. For the clarity of viewing, the optimized structure with no involvement of frontier orbitals is shown at the last figure.

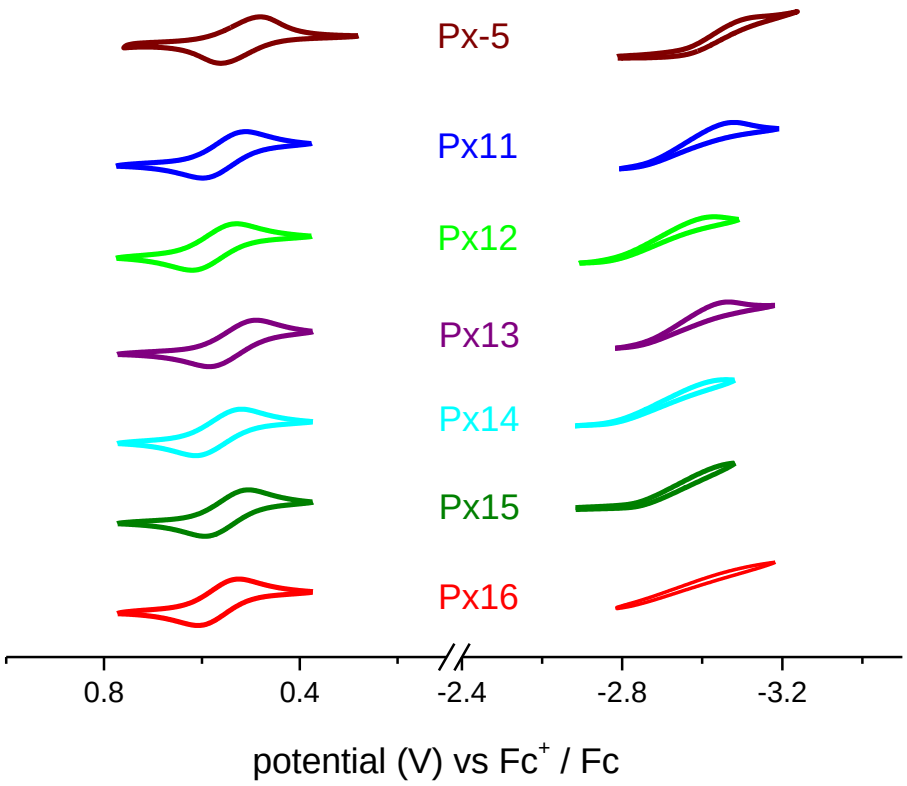

Figure S7. Cyclic voltammetry measurement of the Ir(III) phosphors **Px-11** – **16** for this work.

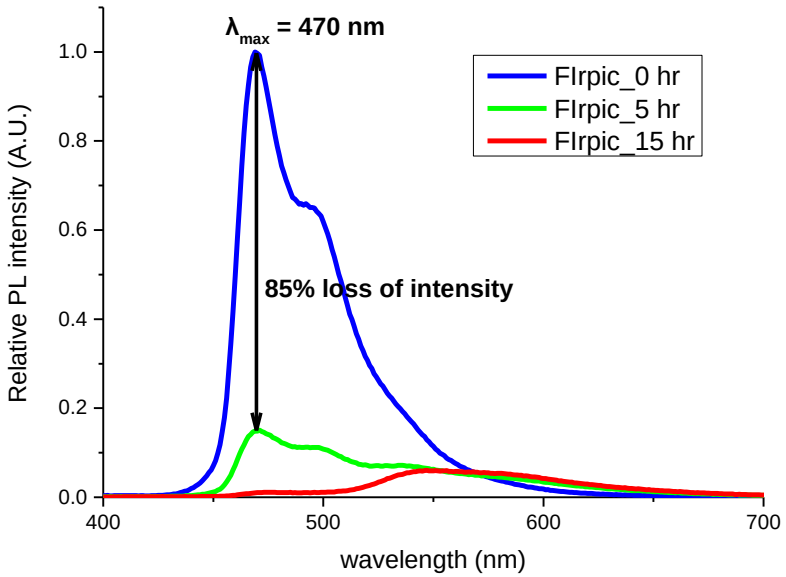

Figure S8. The photo-degradation response of sky-blue emitter, FIrpic, for a period of 15 hrs in degassed toluene.

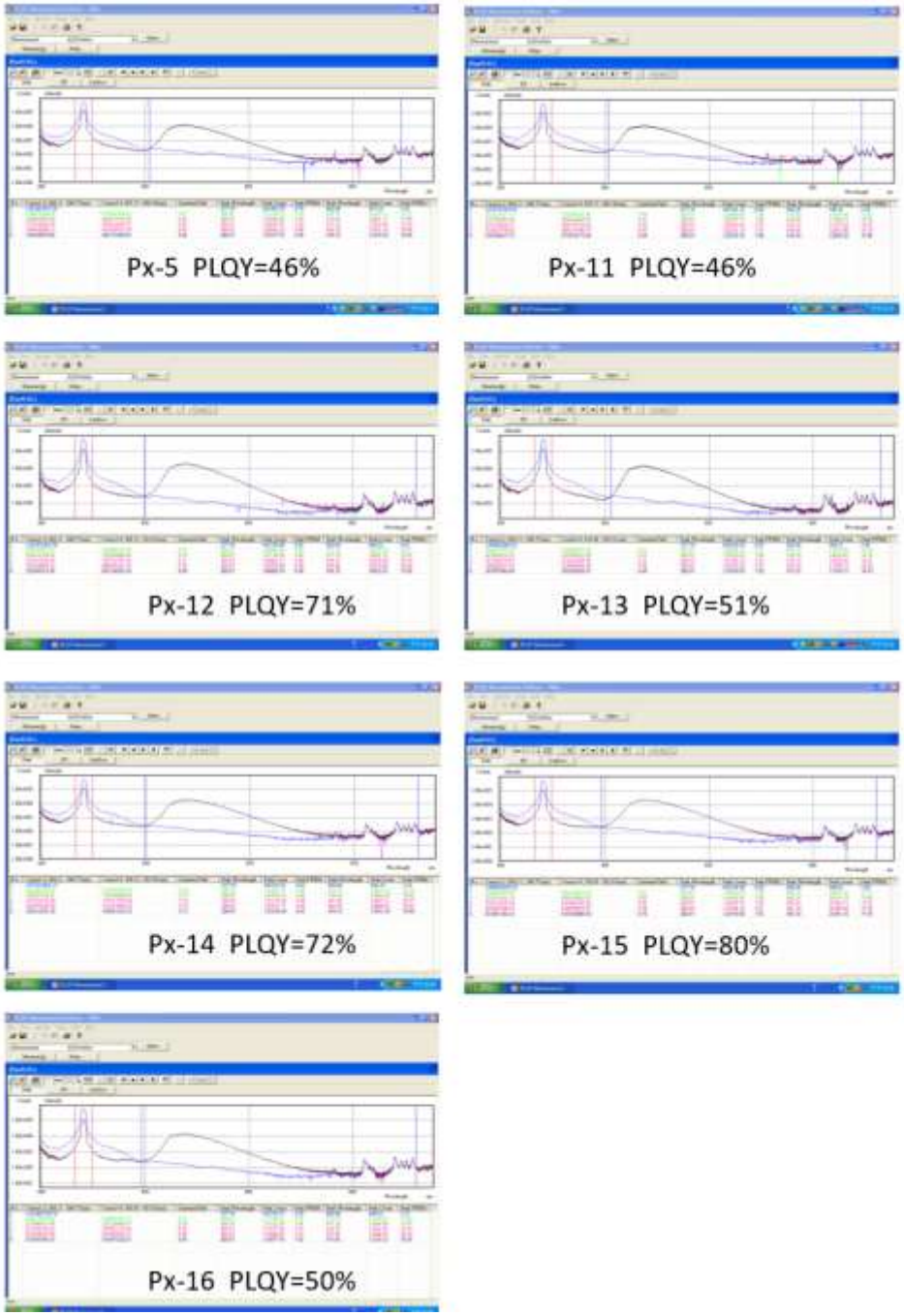

Figure S9. Fluorescence quantum yields (PLQY) for 15 wt.% of Ir(III) dopants in mCPCN. (Absolute PLQY measurements of doped thin films were carried out on a Hamamatsu C9920 system equipped with a xenon lamp, integrating sphere and a model C10027 photonic multi-channel analyzer.)

Table S7. Calculated photodegradation rate constant of the studied Ir(III) dopants.

Dopant	PL λ_{max}	rate constant (hr^{-1})[(a)]	rel. stabilities
fac-[Ir(ppy)$_3$]	510 nm	2.6 x 10^{-3}	100
Px-5	472 nm	1.6 x 10^{-2}	16
Px-11	475 nm	4.6 x 10^{-3}	57
Px-12	472 nm	4.5 x 10^{-3}	58
Px-13	478 nm	5.3 x 10^{-3}	49
Px-14	478 nm	4.3 x 10^{-3}	60
Px-15	473 nm	3.2 x 10^{-3}	81
Px-16	475 nm	2.4 x 10^{-2}	11
mer-[Ir(pmp)$_3$]	419 nm	1.2 x 10^{-2}	22

(a) The rate constants were obtained according to the integrated first-order rate law: $\ln\left[\frac{At}{A0}\right] = -kt$, – slope = rate constant, while relative stability data were calculated in reference to the decomposition rate constant of *fac*-[Ir(ppy)$_3$].

Table S8. Electrochemical data and energy level of Ir(III) metal complexes **Px-11** - **16**.

	$E^{ox}_{½}$ [V] (ΔE_p, V)[(a)]	HOMO [eV][(b)]	Energy gap [eV][(b)]	LUMO [eV][(b)]
Px-5	0.52 (0.08)	−5.32	3.01	−2.31
Px-11	0.55 (0.09)	−5.35	3.01	−2.34
Px-12	0.57 (0.09)	−5.37	2.92	−2.45
Px-13	0.54 (0.09)	−5.34	3.01	−2.33
Px-14	0.57 (0.09)	−5.37	2.91	−2.46
Px-15	0.55 (0.09)	−5.35	2.90	−2.45
Px-16	0.57 (0.08)	−5.37	2.92	−2.45

(a) $E^{ox}_{½}$ refers to [(E_{pa} + E_{pc})/2], where E_{pa} and E_{pc} are the anodic and cathodic wave respectively, for the oxidation half-wave potential and referenced to the ferrocene redox couple (Fc/Fc^+), ΔE_p = $E_{pa} - E_{pc}$ conducted in CH_2Cl_2 solution. (b) HOMO = $|-4.8 - E^{ox}_{½}|$, LUMO = HOMO – energy gap, while energy gap (eV) is calculated from the equation, i.e. 1240/PL onset (in nm).

References

[1] Frisch, M. J.; Trucks, G. W.; Schlegel, H. B.; Scuseria, G. E.; Robb, M. A.; Cheeseman, J. R.; Scalmani, G.; Barone, V.; Mennucci, B.; Petersson, G. A.; Nakatsuji, H.; Caricato, M.; Li, X.; Hratchian, H. P.; Izmaylov, A. F.; Bloino, J.; Zheng, G.; Sonnenberg, J. L.; Hada, M.; Ehara, M.; Toyota, K.; Fukuda, R.; Hasegawa, J.; Ishida, M.; Nakajima, T.; Honda, Y.; Kitao, O.; Nakai, H.; Vreven, T.; Montgomery, J. A.; Peralta, J. E.; Ogliaro, F.; Bearpark, M.; Heyd, J. J.; Brothers, E.; Kudin, K. N.; Staroverov, V. N.; Kobayashi, R.; Normand, J.; Raghavachari, K.; Rendell, A.; Burant, J. C.; Iyengar, S. S.; Tomasi, J.; Cossi, M.; Rega, N.; Millam, J. M.; Klene, M.; Knox, J. E.; Cross, J. B.; Bakken, V.; Adamo, C.; Jaramillo, J.; Gomperts, R.; Stratmann, R. E.; Yazyev, O.; Austin, A. J.; Cammi, R.; Pomelli, C.; Ochterski, J. W.; Martin, R. L.; Morokuma, K.; Zakrzewski, V. G.; Voth, G. A.; Salvador, P.; Dannenberg, J. J.; Dapprich, S.; Daniels, A. D.; Farkas, Ö.; Foresman, J. B.; Ortiz, J. V.; Cioslowski, J.; Fox, D. J. Gaussian 09, Revision D.01. *Gaussian 09, Revision D.01; Gaussian Inc.* **2013**, Wallingford, CT.